Editors' Suggestion | Featured in Physics

Light-Induced Subnanometric Modulation of a Single-Molecule Electron Source

Hirofumi Yanagisawa,[1,2,3,4,*] Markus Bohn,[3] Hirotaka Kitoh-Nishioka,[5] Florian Goschin,[3] and Matthias F. Kling[3,4]

[1]JST, PRESTO, 4-1-8 Honcho, Kawaguchi, Saitama 332-0012, Japan
[2]Institute for Solid State Physics, The University of Tokyo, Chiba 277-8581, Japan
[3]Physics Department, Ludwig-Maximilians-Universität Munich, D-85748 Garching, Germany
[4]Max Planck Institute of Quantum Optics, D-85748 Garching, Germany
[5]Department of Energy and Materials, Faculty of Science and Engineering, Kindai University, Osaka 577-8502 Japan

(Received 15 June 2022; revised 21 November 2022; accepted 18 January 2023; published 8 March 2023)

Single-molecule electron sources of fullerenes driven via constant electric fields, approximately 1 nm in size, produce peculiar emission patterns, such as a cross or a two-leaf pattern. By illuminating the electron sources with femtosecond light pulses, we discovered that largely modulated emission patterns appeared from single molecules. Our simulations revealed that emission patterns, which have been an intractable question for over seven decades, represent single-molecule molecular orbitals. Furthermore, the observed modulations originated from variations of single-molecule molecular orbitals, practically achieving the subnanometric optical modulation of an electron source.

DOI: 10.1103/PhysRevLett.130.106204

Computers consist of an enormous number of switches, namely, transistors. Accelerating and integrating these fundamental devices further are the key for fabricating a next-generation computer. Vacuum nanoelectronics, consisting of a nanoscale object with a counterelectrode as schematically shown in Fig. 1(a), is expected to create electronics faster than modern solid devices [1]. In vacuum electronics, the electron emission from a given object carries the signal. By irradiating such a device with femtosecond light pulses, optical fields localized at the geometrical inhomogeneities of the object, such as a sharp tip, generate ultrafast electron emissions on a timescale of femtoseconds (10^{-15} s) [2–6] or even attoseconds (10^{-18} s) [7–9]. This situation is practically equivalent to a switch with an optically controlled gate, as shown in the lower panel of Fig. 1(a). Thus, ultrafast switches with unprecedented operating speed have been realized. The integration of such a switch in an object then becomes possible. The spatial distribution of the local optical fields can be modulated via plasmonic effects by varying the optical parameters of the laser pulses [4–6,10,11]. Using this method, for instance, the A or B emission sites at the apexes of multiple tips on an object could be selected [5], as in Fig. 1(b). This situation is equivalent to two switches, whose gates can be independently controlled, being integrated into one object. Hence, miniaturizing the optically modulable electron source is key to the further integration of ultrafast vacuum nanoelectronics.

Currently, two emission sites about 10 nm apart can be selected by modulating the local-field distribution [6,12]. Theoretically, it has been predicted that the locations of optical field hotspots can be selected between two atomistic tips a few nanometers apart on a single nano-object [13]. However, as the size of a nano-object approaches 1 nm, it becomes increasingly technically challenging to create multiple tips on an object in a controlled manner [14]. Here, instead of pursuing the optical modulation of local-field distribution, we introduced a new method based on quantum effects that does not require multiple tips, showing that it is possible to miniaturize the optical modulation of an electron source further down to a subnanometric scale.

Our idea was to utilize a resonant electron emission from a solid to a vacuum through a single C_{60} molecule deposited on a solid surface. Upon the resonant emission, the electron transmission rate from the solid to the vacuum is modulated by the local density of the electronic states (LDOS) of the molecule, ρ, namely, the square of a wave function or molecular orbital (MO) at a certain energy level. The electron transmission will be high at a point with a high ρ value [15]. For example, as conceptually depicted in Fig. 1(c), ρ values of the s-type MO in case A are at their maximum at the center of the MO, and thus electron emissions from the center will be prevalent. In contrast, ρ values of the p-type MO in case B reach their highest points at both lobes; thus, the p-type MO provides two emission sites away from the center. These emission sites are located approximately within 1 nm × 1 nm in the case of C_{60}. Supposing one could optically change the MOs through which the emitted electrons pass, e.g., from case A

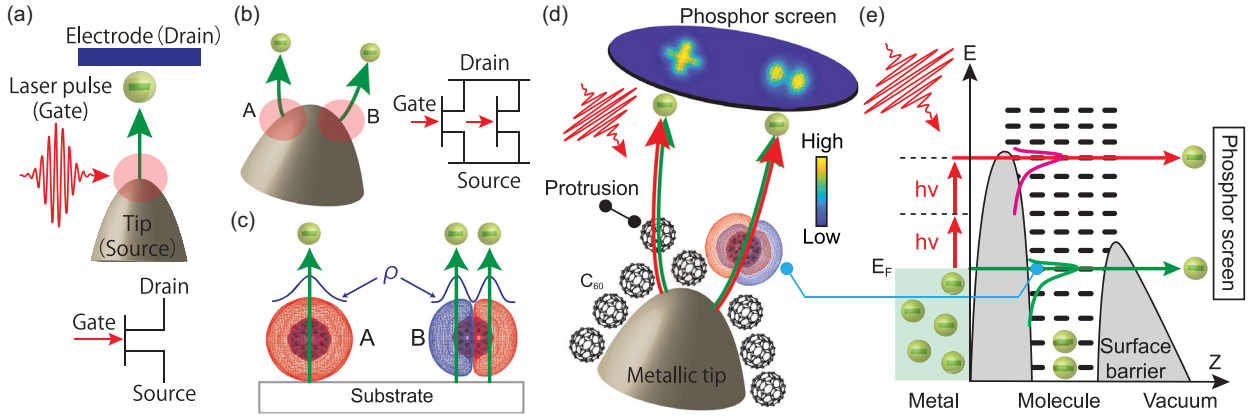

FIG. 1. Conceptual diagram of ultrafast electron emissions from a nano-object by irradiating a light pulse (a) and optical control of emission sites (b). Red solid circles indicate localized optical fields. (c) Conceptual diagram of spatial modulation of an electron source using resonance electron emissions through a molecule. Blue lines indicate the LDOS of the corresponding molecular orbitals, ρ. (d) Schematic of electron emissions from single C_{60} protrusions situated on a molecular layer formed on a sharp metallic tip. (e) Potential energy diagram of possible electron emission mechanisms from a single molecule due to dc electric fields and laser pulse irradiation. In (d) and (e), the green (red) arrows indicate the paths of electrons induced by dc electric fields (laser pulse irradiation) in real space and a potential configuration.

to B. In such a case, one could practically achieve the optical modulation of electron sources on a subnanometric scale.

For the demonstration of our proposed idea, we used a single-molecule electron source. By applying strong direct-current (dc) electric fields to C_{60} molecules deposited on a tip with a radius curvature of a few hundred nanometers, we identified that some single-molecule-terminated protrusions appeared on a molecular layer formed on the tip, as depicted in Fig. 1(d) [16]. In this case, the electric fields became stronger at the protrusions, and the strong fields drove electron emissions from these individual molecules. The emitted electrons radially propagated from the apex and magnified nanoscopic information [17]. Then, the observation of the emission patterns projected on a phosphor screen can serve as a form of electron microscopy, known as field emission microscopy (FEM). Notably, the electrons emitted from single molecules show peculiar patterns, such as a cross or a two-leaf pattern, as shown in Fig. 1(d). These patterns sometimes change over time—for example, from a two-leaf pattern to a cross pattern. These peculiar patterns and their variations were first observed around 70 years ago [18]. However, no satisfactory theoretical model has yet been developed to explain the formation mechanism of the patterns, mainly because of the lack of information on molecular arrangements on a metallic needle [17–23].

Our previous work showed that a protrusion molecule sticks out from a large vacant space in the monolayer and there is no molecule beneath the protrusion molecule, as schematically drawn in Fig. 1(d) [16,24]. In such a configuration, we expect resonant electron emissions where the emitted electrons originate from the substrate metal and pass through only the protrusion molecules before emission, as depicted by the green arrows in Fig. 1(d) [25]. A potential emission mechanism corresponding to the proposed emission process is shown in Fig. 1(e). In this figure, the surface barrier (gray area) is bent by a strong dc electric field at the tip apex, allowing electrons to leak from the Fermi level of the substrate metal via tunneling. After passing through an unoccupied molecular level, the electrons are emitted into a vacuum and move up to a screen, as indicated by the green arrow [17]. Here, the electron transmission rate from the substrate to the vacuum would be modulated via the LDOS of the MO through which the electron passes [15]. As a result, the emission patterns would reflect the shapes of the molecular orbitals. For example, in the case of a p-type orbital, as shown in Fig. 1(d), the emission pattern would resemble a two-leaf pattern.

By illuminating the single-molecule electron source and inducing the photoexcited electron emissions [28], we expect to realize the MO change, as outlined in Fig. 1(c). The previous study showed that laser-induced electrons are emitted mainly via the two-photon photoexcitation (2PPE) level at around the threshold tip voltage when dc-field emission can begin to be observed, as depicted by the red arrows in Fig. 1(e) [29–31]. In this case, the photoexcited electron should be resonantly emitted through the MO at the 2PPE level. Because the symmetry of MOs drastically changes with their discrete energy levels [40], a drastic change in emission patterns would be expected with respect to the patterns induced by dc electric fields, the signature of achieving the subnanometric optical modulation of electron emissions.

To demonstrate our idea, we performed FEM and laser-induced FEM (LFEM) experiments. We used the same experimental setup as in our previous work [16]. A tungsten

tip oriented toward the [011] direction was installed in the ultrahigh vacuum chamber (1×10^{-10} mbar). The fullerene molecules were evaporated by resistively heating the boat and then deposited onto the tip apex. In the FEM experiments, the emission patterns projected onto a phosphor screen were recorded using a CCD camera. In front of the screen (tip side), a metallic mesh was installed. The phosphor screen and the mesh were grounded, and a tip was negatively biased to perform the FEM experiments. In the LFEM experiments, a chevron-type microchannel plate was installed between the phosphor screen and the metallic mesh. Laser pulses were generated by an oscillator (center wavelength: 830 nm; repetition rate: 80 MHz; and pulse duration: sub-10 fs, linear polarization) and introduced into a vacuum chamber. A spherical mirror with a focal length of 30 mm in the chamber focused the laser to approximately 10.1 μm diameter ($1/e^2$ radius) onto the tip apex. The laser fluence was around 0.35–0.4 mJ/cm^2 [41].

By illuminating C_{60} molecules on the tip, we succeeded in inducing electron emissions from a single molecule and observed large modulations in their patterns as we have outlined above. We observed the emission patterns of round spots without light irradiation, as shown in the upper panels of Figs. 2(a) and 2(c). In contrast, the laser-induced emission patterns showed drastic changes, and ring or two-leaf patterns appeared, as shown in the lower panel of each figure [44]. The laser-induced patterns could be repeatedly observed by turning the light on and off. We did not observe noticeable pattern changes before and after the illumination. An example of the sequential changes of patterns from another molecule is shown in Fig. 2(e). The first and fourth images show dc-field-induced spot patterns. The second and fifth represent laser-induced ringlike patterns, where no dc-field-driven signals could be observed due to the low tip voltage (see the third and sixth images without illumination). These patterns did not change during the two cycles. In the fifth ringlike pattern of Fig. 2(e), we slightly increased the laser power by a factor of 1.15 with respect to that of the second pattern. The total laser-induced signal increased by a factor of 1.32 from the second to the fifth patterns. This value was consistent with the 2PPE process, as the signal should increase with the square of the laser intensity, namely $1.15^2 = 1.32$.

Based on the scenario described in Fig. 1(e), the present study developed a simulation model for clarifying the emission patterns from a single molecule. First, the MOs and their energies in a single molecule were simulated under an external dc electric field based on density functional theory (DFT) using GAMESS software [45], without a substrate or other molecules. In the simulations, geometric optimizations were first performed using the B3LYP-D3BJ/6-31G(d) as functional and basis set [46–48]. Thereafter, single-point B3LYP/6–31 + G(d) [49] calculations were performed to obtain MOs and their MO energies. Using the visualization software

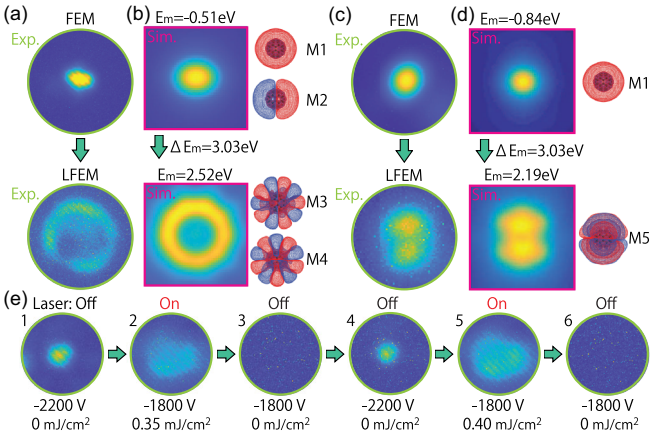

FIG. 2. (a),(c) Observed electron emission patterns from single molecules without (upper panel) and with (lower panel) irradiation of femtosecond light pulses. Tip voltages of the upper and lower panels are (a) −800 and −600 V, and (b) −2800 and −2200 V. The laser fluence was 0.35 mJ/cm^2. (b) and (d) Simulations corresponding to the observations in (a) and (c), respectively. They are done under dc electric fields of 5.14 V/nm [17]. The front views of the molecular orbitals of the main contributors to each emission pattern are also shown in (b) and (d). The molecular energy levels of orbitals M1, M2, M3, M4, and M5 are −0.912, −0.340, 2.571, 2.580, and 2.204 eV, respectively. (e) The sequential changes in emission patterns with and without laser excitation. Tip voltage and laser fluence are shown with each pattern. The polarization vector was parallel to the tip axis in (a) and (c), but in (e), the vector was rotated by 45° from the tip axis in a clockwise direction when the laser beam propagated toward the tip apex.

MacMolplt [50], three-dimensional grid data of the MOs in the range of 30 for the X, Y, and Z with 128 data points for each axis were extracted from the GAMESS output. From the calculated MOs, we extracted the wave functions greater than 1 nm from the center of a molecule. The wave functions in this area were in a vacuum, namely, they were the emitted electrons. The extracted wave functions were then propagated onto a screen using the formula provided in Ref. [51]. The emission pattern is thus a map of the intensities of the far-field wave function integrated along the perpendicular axis to the screen. In these simulations, the distance between the tip and the screen was 23 mm, and the voltage between them was 3000 V. These parameters were in line with the experimental conditions. The resulting emission patterns were blurred by assuming a spatial resolution of 0.3 nm, as predicted for single-molecule FEM patterns [19]. The magnifications of the simulated emission patterns were determined by assuming that the size of a pattern for the lowest unoccupied MO represents the MOs around 1 nm.

In the resonant emission process, after the electrons in the substrate have tunneled through the surface barrier, the electrons should have an asymmetric energy distribution with a peak situated at the Fermi level [29], as indicated by the green lines in Fig. 1(e). Given the finite energy width of the energy spectrum, emitted electrons pass through

several MOs. Hence, the observed emission patterns are a superposition of the emission patterns arising from the MOs involved [52]. The weight of each MO contributing to a given emission was determined by the asymmetric energy distribution, for which we assumed a typical energy spectrum observed after tunneling via dc electric fields [29]. Note that the far-field wave functions were incoherently superimposed, while coherent superposition did not match our observations. In this simulation, because we calculated only single-molecule MOs in the DFT simulations, we did not know which molecular energy level was situated around the Fermi level of the substrate. Therefore, we simulated the emission patterns by gradually shifting the entirety of the molecular levels with respect to the Fermi level. Here, we defined the molecular energy, E'_m, as the electron energy in a single molecule that was obtained by GAMESS software and E_m as E'_m situated at the Fermi level [53]. We investigated how the emission patterns changed with varying E_m for different molecular geometries and dc electric fields. The resulting images were compared with our observations.

First, we applied our simulation model to clarify the interpretation of the peculiar emission patterns generated by dc electric fields and reveal the underlying physics of the most mysterious behavior of emission patterns, specifically the dramatic pattern changes that occur over time. The upper panels of Figs. 3(a), 3(d) display some series of pattern variations. These pattern variations were understood as caused by a thermal fluctuation in molecular positions because pattern variations were suppressed at approximately 80 K [20]. It is tempting to associate these patterns with molecular or atomic configurations and to attribute the changes to a reconfiguration of some molecules or to a change in the bonding geometry of a single molecule from, e.g., standing up to lying down [17,18,20–22]. However, none of these ideas has provided a consistent explanation [23,54]. In contrast, our simulation model consistently reproduced those emission patterns, as shown in the lower panels of Figs. 3(a)–3(d) [55]. In these simulations, we employed the C_{60} geometry shown in Fig. 3(e). The different patterns can be obtained from the same C_{60} geometry because the main contributing MOs in the patterns change along with E_m values. Furthermore, we discovered that the observed pattern variations could be reproduced by emission patterns with nearby E_m values. As shown in Figs. 3(a)–3(d), the E_m values were very close, ranging from 0.04 to 0.35 eV. Based on such excellent agreement, we concluded that thermal fluctuation drives the shifts in their E_m values and the subsequent changes in emission patterns.

We hypothesize that the thermal fluctuation causing these energy shifts could be an extremely small displacement of the molecule along the vertical axis of the surface. This idea can be explained via the simplified potential diagram shown in Fig. 3(f). Assuming that we have two

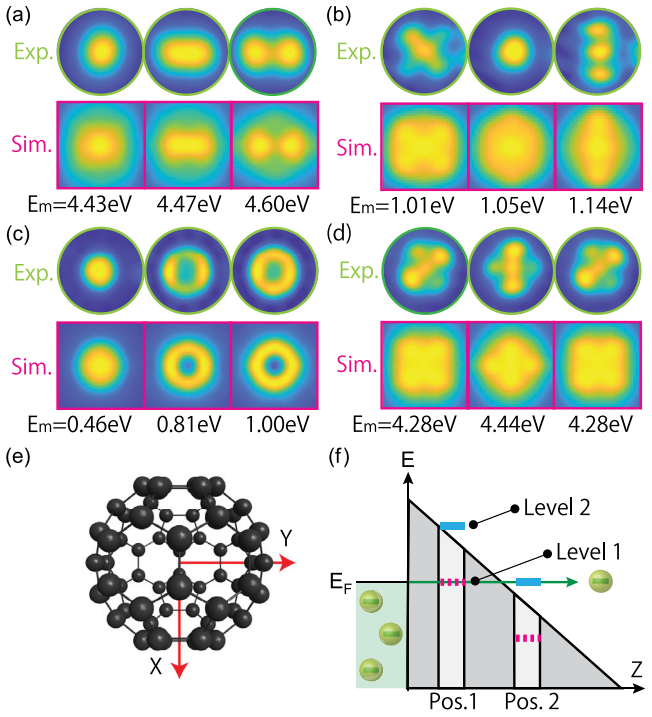

FIG. 3. (a)–(d) Variations of observed electron emission patterns from a variety of single molecules (upper panels) and simulated results from a single fullerene molecule (lower panels) via dc electric fields. Tip voltages are (a) −3000 V, (b) −2600 V, (c) −3000 V, and (d) −4200 V. In the observed images, the shadow images from the metallic mesh, as can be seen in the emission patterns in Fig. 1(d), were removed using a fast Fourier transform filter. Simulations are done under dc electric fields of 6.17 V/nm for (a) and (c), and 5.14 V/nm for (b) and (d). (e) The geometry of C_{60} used in the simulation together with the X and Y vectors of the Cartesian coordinate axes. The vector of the z axis is directed towards the readers (not shown). The electric fields were applied along the z axis so that the electrons were emitted toward the reader. (f) Conceptual diagram for a change of molecular orbitals to be observed in emission patterns from a single molecule.

levels in a molecule situated at position 1, with level 1 at the same height as the Fermi level, we should see the MO in level 1 in the FEM emission pattern. If the molecule moves vertically to the surface and shifts to position 2, these levels should move down following the dc electric potential. If level 2 moves down to the Fermi level of the metal when the molecule is at position 2, one should see the MO of level 2. As a result, we should see a sudden change in emission patterns. A quick estimation of the amount of vertical displacement can be done by assuming dc fields of 5 V/nm, which was the typical value obtained in our simulations [56]. Only 0.1 to 0.7 Å were required to experience a change from 0.04 to 0.35 eV [57].

Next, we applied our simulation model to the light-induced emission patterns. As discussed above and shown in Fig. 1(e), the light-induced emission should represent

the MOs approximately 3 eV above the Fermi level, while the pattern without light irradiation represented the MOs around the Fermi level. Hence, in our simulations, we searched for sets of two emission patterns that had a molecular energy gap of about 3 eV and matched our observations. We successfully found such combinations, as shown in Figs. 2(b) and 2(d). These simulations correspond to the observed images presented in Figs. 2(a) and 2(c), respectively. For example, in Fig. 2(a), the emission pattern without light is slightly oval, and the ring pattern in the light-induced pattern is asymmetric. Even these details were reproduced in the simulations [60]. Also, the main characteristics of the emission patterns reflected the shapes of the molecular orbitals of the main contributors, which are shown beside the simulated emission patterns. For example, the oval spot in Fig. 2(b) originated from the superposition of *s*-type and *p*-type orbitals. The ring pattern originated from flowerlike orbitals. In this case, the FEM spatial resolution of 0.3 nm smeared out the detailed structures of the petals, thus resulting in the ring pattern. Based on the excellent agreement, we conclude that MOs at the 2PPE level in a single C_{60} molecule were observed. Because the pattern changes were driven by the MO variation, we practically achieved the subnanometric optical modulation of an electron source, as depicted in Fig. 1(c).

In this Letter, we introduced a new concept to spatially modulate a single-molecule electron source using quantum effects and experimentally demonstrated the concept. This concept would facilitate the creation of an electron source with optically controlled emission sites on an atomic scale, integrating ultrafast switches into a single molecule. In addition, the electron emission from a single molecule on a tip can be used as a microscope. Our simulations revealed that FEM molecular images represent MOs in a single molecule. Using FEM together with the simulations, the molecular orientation and the energy levels of the observed MOs could be identified, and thereby the physics of pattern variations due to thermal fluctuation were revealed in this study. Furthermore, we have shown that LFEM visualizes single-molecule MOs at photoexcited levels at an unprecedented submolecular resolution [62]. Because the LFEM employs femtosecond light pulses, using it to observe ultrafast hot electron dynamics would be straightforward [29]. The hot electron dynamics in a single molecule play a significant role in molecular devices [63–67] and even natural phenomena such as photosynthesis [68]. Hence, LFEM would be useful for exploring microscopic electron dynamics in these systems.

This work was supported by the Murata Science Foundation, the Sumitomo Foundation (Grant No. 180920), Research Foundation for Opto-Science and Technology, the Precise Measurement Technology Promotion Foundation (PMTP-F), the Research Center for Biomedical Engineering, Japan Science and Technology Agency via PRESTO project (Grant No. 1082208), the PETACom project financed by the European Research Council via the FET Open H2020 program, the Deutsche Forschungsgemeinschaft (DFG, German Research Foundation) via DFG project funding (Project No. 389759512). We acknowledge many useful discussions with Professor Jürg Osterwalder, Professor Neo Yoichi, Mr. Hiroki Sannohe, Professor Thomas Greber, Professor Marcelo Ciappina, Professor Fumio Komori, Professor Yoichi Yamada, Ms. Jessica Zauner, and Dr. Johannes Schötz.

*hirofumi.yanagisawa@issp.u-tokyo.ac.jp

[1] J. W. Han, J. S. Oh, and M. Mayyappan, Vacuum nanoelectronics: Back to the future? Gate insulated nanoscale vacuum channel transistor, Appl. Phys. Lett. **100**, 213505 (2012).

[2] P. Hommelhoff, Y. Sortais, A. Aghajani-Talesh, and M. A. Kasevich, Field Emission Tip as a Nanometer Source of Free Electron Femtosecond Pulses, Phys. Rev. Lett. **96**, 077401 (2006).

[3] T. Higuchi, L. Maisenbacher, A. Liehl, P. Dombi, and P. Hommelhoff, A nanoscale vacuum-tube diode triggered by few-cycle laser pulses, Appl. Phys. Lett. **106**, 051109 (2015).

[4] M. Aeschlimann, M. Bauer, D. Bayer, T. Brixner, F. J. García de Abajo, W. Pfeiffer, M. Rohmer, C. Spindler, and F. Steeb, Adaptive subwavelength control of nano-optical fields, Nature (London) **446**, 301 (2007).

[5] P. Melchior, D. Bayer, C. Schneider, A. Fischer, M. Rohmer, W. Pfeiffer, and M. Aeschlimann, Optical near-field interference in the excitation of a bowtie nanoantenna, Phys. Rev. B **83**, 235407 (2011).

[6] H. Yanagisawa, C. Hafner, P. Doná, M. Klckner, D. Leuenberger, T. Greber, M. Hengsberger, and J. Osterwalder, Optical Control of Field-Emission Sites by Femtosecond Laser Pulses, Phys. Rev. Lett. **103**, 257603 (2009).

[7] M. Krueger, M. Schenk, and P. Hommelhoff, Attosecond control of electrons emitted from a nanoscale metal tip, Nature (London) **475**, 78 (2011).

[8] B. Förg *et al.*, Attosecond nanoscale near-field sampling, Nat. Commun. **7**, 11717 (2016).

[9] M. Ludwig, G. Aguirregabiria, F. Ritzkowsky, T. Rybka, D. C. Marinica, J. Aizpurua, A. G. Borisov, A. Leitenstorfer, and D. Brida, Sub-femtosecond electron transport in a nanoscale gap, Nat. Phys. **16**, 341 (2020).

[10] H. Yanagisawa, C. Hafner, P. Doná, M. Klöckner, D. Leuenberger, T. Greber, J. Osterwalder, and M. Hengsberger, Laser-induced field emission from a Tungsten tip: Optical control of emission sites and the emission process, Phys. Rev. B **81**, 115429 (2010).

[11] H. Yanagisawa, T. Greber, C. Hafner, and J. Osterwalder, Laser-induced field emission from a tungsten nano-tip by circularly-polarized femtosecond laser pulses, Phys. Rev. B **101**, 045406 (2020).

[12] H. Yanagisawa, M. Ciappina, C. Hafner, J. Schötz, J. Osterwalder, and M. F. Kling, Optical control of Youngs type double-slit interferometer for laser-induced electron emission from a nano-tip, Sci. Rep. **7**, 12661 (2017).

[13] M. Urbieta, M. Barbry, Y. Zhang, P. Koval, D. Sánchez-Portal, N. Zabala, and J. Aizpurua, Atomic-scale lightning rod effect in plasmonic picocavities: A classical view to a quantum effect, ACS Nano **12**, 585 (2018).
[14] G. Cárdenas-Triviño, R. A. Segura, and J. Reyes-Gasga, Palladium nanoparticles from solvated atomsstability and HRTEM characterization, Colloid Polym Sci. **282**, 1206 (2004).
[15] J. W. Gadzuk, Single-atom point source for electrons: Field-emission resonance tunneling in scanning tunneling microscopy, Phys. Rev. B **47**, 12832 (1993).
[16] H. Yanagisawa, M. Bohn, F. Goschin, A. P. Seitsonen, and M. F. Kling, Field emission microscopy for a single fullerene molecule, Sci. Rep. **12**, 2174 (2022).
[17] R. Gomer, *Field Emission and Field Ionization* (American Institute of Physics, New York, 1993).
[18] E. W. Müller, Z. Die Sichtbarmachung einzelner Atome und Molekle im Feldelektronenmikroskop, Naturforschung **5a**, 473 (1950).
[19] D. J. Rose, On the magnification and resolution of the field emission electron microscope, J. Appl. Phys. **27**, 215 (1956).
[20] A. J. Melmed and E. W. Müller, Study of molecular patterns in the field emission microscope, J. Chem. Phys. **29**, 1037 (1958).
[21] J. A. Becker and R. G. Brandes, On the adsorption of oxygen on Tungsten as revealed in the field emission electron microscope, J. Chem. Phys. **23**, 1323 (1955).
[22] T. A. Tumareva, G. G. Sominskii, and A. S. Polyakov, Formation on field emitters coated with fullerenes of microformations producing ordered emission images, Tech. Phys. **47**, 250254 (2002).
[23] Y. Neo, T. Matsumoto, M. Tominita, M. Sasaki, and H. Mimura, Necessary conditions for two-lobe patterns in field emission microscopy, J. Appl. Phys. **51**, 115601 (2012).
[24] See Supplemental Material at http://link.aps.org/supplemental/10.1103/PhysRevLett.130.106204 for Sec. I. Reference [16] shows that there are three different types of configurations regarding protrusion molecules.
[25] The momentum distribution of field-emitted electrons is narrowly distributed around the axis normal to the surface. Because of this property, the paths of the electrons emitted at the top of the protrusion molecule should be limited to the space between the protrusion and the substrate. See Sec. II of the Supplemental Material [24], which includes Ref. [26,27].
[26] R. D. Young, Theoretical total-energy distribution of field-emitted electrons, Phys. Rev. **113**, 110 (1959).
[27] T. A. de Assis, F. F. DallAgnol, and R. G. Forbes, Field emitter electrostatics: A review with special emphasis on modern high-precision finite-element modelling, J. Phys. Condens. Matter **34**, 493001 (2022).
[28] Y. Gao and R. Reifenberger, Photofield emission from transition-metal surface states, Phys. Rev. B **35**, 4284 (1987).
[29] H. Yanagisawa, M. Hengsberger, D. Leuenberger, M. Klöckner, C. Hafner, T. Greber, and J. Osterwalder, Energy Distribution Curves of Ultrafast Laser-Induced Field Emission and Their Implications for Electron Dynamics, Phys. Rev. Lett. **107**, 087601 (2011).
[30] M. Duchet, S. Perisanu, S. T. Purcell, E. Constant, V. Loriot, H. Yanagisawa, M. F. Kling, F. Lepine, and A. Ayari, Femtosecond laser induced resonant tunneling in an individual quantum dot attached to a nanotip, ACS Photonics **8**, 505 (2021).
[31] DFT simulations based on simplified models showed that the top of the potential barrier was around 3 eV above the Fermi level. See Sec. III of the Supplemental Material [24], which includes Ref. [32–39].
[32] N. R. Gall, E. V. Rutkov, and A. Y. Tontegode, Interaction of C_{60} molecules with the (100)W surface: Adsorption, initial stages of film growth, and thermal transformation of the adsorption layer, Semiconductors **38**, 10231029 (2004).
[33] K.-D. Tsuei, J. Y. Yuh, C. T. Tzeng, R. Y. Chu, S. C. Chung, and K. L. Tsang, Photoemission and photoabsorption study of C_{60} adsorption on Cu(111) surfaces, Phys. Rev. B **56**, 15412 (1997).
[34] I. Hamada, van der Waals density functional made accurate, Phys. Rev. B **89**, 121103(R) (2014).
[35] L. Bengtsson, Dipole correction for surface supercell calculations, Phys. Rev. B **59**, 12301 (1999).
[36] P. Giannozzi *et al.*, QUANTUM ESPRESSO: A modular and open-source software project for quantum simulations of materials, J. Phys. Condens. Matter **21**, 395502 (2009).
[37] P. Giannozzi *et al.*, Advanced capabilities for materials modelling with QUANTUM ESPRESSO, J. Phys. Condens. Matter **29**, 465901 (2017).
[38] J. P. Perdew, K. Burke, and M. Ernzerhof, Generalized Gradient Approximation Made Simple, Phys. Rev. Lett. **77**, 3865 (1996).
[39] B. M. Hall, S. Y. Tong, and D. L. Mills, Large-Angle Electron-Energy-Loss Spectroscopy with the Inclusion of a Surface Image Potential, Phys. Rev. Lett. **50**, 1277 (1983).
[40] M. Feng, J. Zhao, and H. Petek, Atomlike, Hollow-CoreBound Molecular Orbitals of C_{60}, Science **320**, 359 (2008).
[41] Under the optical parameters used in our experiments, thermionic emissions from a tungsten tip, which occur on the scale of a picosecond or even slower, are unlikely, and the electron emission will occur within the sub-10 fs laser envelope [42]. Thus the emitted electrons will not see transient changes in molecular positions that may occur when phononic systems are heated, typically a couple of hundreds of femtoseconds after the laser excitation [43].
[42] H. Yanagisawa, S. Schnepp, C. Hafner, M. Hengsberger, D. E. Kim, M. F. Kling, A. Landsman, L. Gallmann, and J. Osterwalder, Delayed electron emission in strong-field driven tunnelling from a metallic nanotip in the multi-electron regime, Sci. Rep. **6**, 35877 (2016).
[43] M. Lisowski, P. A. Loukakos, U. Bovensiepen, J. Sthler, C. Gahl, and M. Wolf, Ultra-fast dynamics of electron thermalization, cooling and transport effects in Ru(001), Appl. Phys. A **78**, 165 (2004).
[44] Note that we reduced the tip voltages in the case of laser-induced electron emission to suppress the strong electron emission components caused by the dc fields. Hence, the signals in LFEM images are all photoexcited electrons. We observed the same combination of dc-field and laser-induced emission patterns when the dc-field components were not suppressed. Hence, we evaluated the simulations at

the constant dc fields in Figs. 2(b) and 2(d). See Sec. IV of the Supplemental Material [24].

[45] G. M. J. Barca *et al.*, Recent developments in the general atomic and molecular electronic structure system, J. Chem. Phys. **152**, 154102 (2020).

[46] A. D. Becke, Density-functional thermochemistry. III. The role of exact exchange, J. Chem. Phys. **98**, 5648 (1993).

[47] S. Grimme, J. Antony, S. Ehrlich, and H. Krieg, A consistent and accurate *ab initio* parametrization of density functional dispersion correction (DFT-D) for the 94 elements H-Pu, J. Chem. Phys. **132**, 154104 (2010).

[48] S. Grimme, S. Ehrlich, and L. Goerigk, Effect of the damping function in dispersion corrected density functional theory, J. Comput. Chem. **32**, 1456 (2011).

[49] J. O. Johansson, G. Henderson, F. Remacle, and E. E. B. Campbell, Angular-Resolved Photoelectron Spectroscopy of Superatom Orbitals of Fullerenes, Phys. Rev. Lett. **108**, 173401 (2012).

[50] B. M. Bode and M. S. Gordon, MacMolPlt: A graphical user interface for GAMESS, J. Mol., Graph. Model. **16**, 133 (1999).

[51] T. Lukes and T. S. Somaratna, The exact propagator for an electron in a uniform electric field and its application to Stark effect calculations, J. Phys. C **2**, 586 (1969).

[52] Examples of emission patterns and their contributing MOs can be found in Sec. V of the Supplemental Material [24].

[53] A schematic illustration of the definition of E_m is available in Sec. VI of the Supplemental Material [24].

[54] T. Matsumoto, T. Nakamura, Y. Neo, H. Mimura, and M. Tomita, *Graphene Simulation* (InTech, Croatia, 2011), Chap. 8.

[55] The propagator that calculates a far-field wave function at the screen from a wave function just after tunneling emission from a single molecule assumes a constant electric field [51]; in reality, however, electric fields are strong around the tip apex and become weaker toward the screen. The discrepancy would lead to blunter images in the simulations compared to the experimental ones.

[56] The strengths of electric fields at the protrusions that we obtained in our previous work [16] ranged from 3 to 4 V/nm. Although the previous work underestimated the field enhancement effect, the field values were close to those we obtained in the present work.

[57] DFT simulations based on simplified models and molecular dynamics simulations have also shown similar results. See Sec. VII of the Supplemental Material [24], which includes Ref. [58,59].

[58] H. J. C. Berendsen, J. P. M. Postma, W. F. van Gunsteren, A. DiNola, and J. R. Haak, Molecular dynamics with coupling to an external bath, J. Chem. Phys. **81**, 3684 (1984).

[59] A. J. Melmed and E. W. Müller, Study of molecular patterns in the field emission microscope, J. Chem. Phys. **29**, 1037 (1958).

[60] The reason the ringlike patterns in Fig. 2(e) were blunter than that of Fig. 2(a) is the difference in the molecular configurations. See Sec. VIII of the Supplemental Material [24], which includes Ref. [61].

[61] H. Yanagisawa, Site-selective field emission source by femtosecond laser pulses and its emission mechanism, Ann. der Phys **525**, 126 (2012).

[62] M. Dąbrowski, Y. Dai, and H. Petek, Ultrafast photoemission electron microscopy: Imaging plasmons in space and time, Chem. Rev. **120**, 6247 (2020).

[63] M. Brongersma, N. Halas, and P. Nordlander, Plasmon-induced hot carrier science and technology, Nat. Nanotechnol. **10**, 2534 (2015).

[64] J. Zhou, K. Wang, and Y. Dubi, Photoconductance from exciton binding in molecular junctions, J. Am. Chem. Soc. **140**, 7073 (2018).

[65] Y. Zeng, J. Chen, T. Yu, G. Yang, and Y. Li, Molecular-supramolecular light harvesting for photochemical energy conversion: Making every photon count, ACS Energy Lett. **2**, 357 (2017).

[66] K. Trofymchuk, A. Reisch, P. Didier *et al.*, Giant light-harvesting nanoantenna for single-molecule detection in ambient light, Nat. Photonics **11**, 657663 (2017).

[67] Z. Q. You and C. P. Hsu, Theory and calculation for electronic coupling in excitation energy transfer, Int. J. Quantum Chem. **114**, 102115 (2013).

[68] R. Cogdell, A. Gall, and J. Köhler, The architecture and function of the light-harvesting apparatus of purple bacteria: From single molecules to *in vivo* membranes, Q. Rev. Biophys. **39**, 227 (2006).